Changyong Jiang and Lixi Huang (2020). Realization of equivalent gradience of porous materials with periodic macro void structure. *Mechanical Systems and Signal Processing*

doi:10.1016/j.ymssp.2019.106434

Realization of equivalent gradience of porous materials with periodic macro void structure

Changyong Jiang

Lixi Huang

Submitted to *Mechanical Systems and Signal Processing* May 12 2019

Accepted October 10 2019

Realization of equivalent gradience of porous materials with periodic macro void structure

Abstract

In this paper, a periodic macro void (PMV) design of porous materials is proposed, through which different acoustic properties can be obtained with uniform porous materials. The proposed PMV structure is an alternative to realize gradient sound absorbers, which experimentally shows the potential to enhance the sound absorption performance of porous materials. Based on the wave finite element (WFE) method and a homogenization procedure, the equivalent density and bulk modulus of PMV porous materials are obtained, which are validated by finite-unit's simulation and experiment. These equivalent acoustic parameters are between that of uniform porous materials and air, which are controlled by the macro porosity, but independent of void position and shape. The proposed PMV porous material with gradient macro voids is used to optimize the anechoic chamber performance with an optimization procedure provided. For a chamber with size of 9 m × 8 m × 7 m, and cut-off frequency of 100 Hz, the performance of gradient PMV design is compared with the classic wedge design. It is found that the optimized gradient PMV design can achieve better performance than the classic wedge design with the same thickness of 0.8 *m*. Moreover, the thickness of gradient PMV design can be reduced up to 15% (0.68 *m*) while keeping better performance than the wedge design.

Keywords: Periodic macro void; Porous materials; Eigenmode; Homogenization; Gradient design; Anechoic chamber

1 Introduction

Acoustic wave propagating in periodic structures has been investigated extensively in recent years. Periodic structures are often formed with periodic boundaries or periodic scatterers inside a uniform material.

Physical behaviors of the acoustic wave in periodic structures can be characterized in different frequency ranges. In the high-frequency range, bandgaps caused by Bragg resonance can be found [1, 2], while in the low-frequency range, homogenization process can be conducted to obtain equivalent acoustic parameters of the periodic structure. Bai and Keller found the decreased phase velocity in the low-frequency range for wave propagating in a waveguide with periodic embedded rigid spheres [3]. Krokhin et al. also found the decreased speed of sound in periodic elastic composites [4]. Jiang and Huang proposed a periodic corrugated waveguide (PCWG) structure, which also shows the decreased speed of sound in the low-frequency range [5]. It was found that the decreased speed of sound was caused by increased equivalent mass while the equivalent bulk modulus of the system was kept unchanged. Therefore, the equivalent parameters of a material can be changed with different inside periodic arrangements in the low-frequency range. In other words, the acoustic properties of the material can be adjusted with different inside periodic scatterers. Many researchers have made their efforts to improve the sound absorption performance of materials by embedding different scatterers inside, which can be hard inclusions, resonant inclusions, void inclusions and so on.

Groby et al. investigated the sound absorption performance of a rigid-frame porous plate with a periodic set of high-contrast inclusions. It was found that the sound absorption was increased due to the excitation of modified modes of plate by the inclusions [6]. Later on, Groby et al. further studied the absorption performance of rigid-frame porous materials with rigid inclusions, and they found absorption peaks below the quarter-wavelength resonance frequency, which was attributed to the excitation of additional modes caused by rigid inclusions [7-9]. Sharma el al. further studied sound absorption by a viscoelastic medium with periodic hard inclusions [10]. A homogenization procedure was also provided by Sharma el al. to replace the whole structure by a uniform medium with equivalent acoustic properties. High sound absorption was observed, which was attributed to dipole resonance and scatters of the hard inclusions.

In addition to hard inclusions, effect of resonant inclusions inside porous materials has also been studied. Boutin investigated the acoustic performance of rigid-frame porous materials with inner resonators [11]. A broad bandgap along with strongly dispersed waves was observed and analyzed with characteristics of the porous matrix and inner resonators. In Lagarrigue et al.'s study, low-frequency performance improvement of porous materials with periodic resonant inclusions was observed [12]. It was demonstrated by Boutin and Becot that inner resonators in porous materials may change the equivalent acoustic properties of the porous material

significantly [13]. Groby et al. investigated sound absorption of porous foam with embedded Helmholtz Resonators (HRs) [14]. It was found that the absorption coefficient for low frequencies near HR excitation was enhanced, which was due to the excitation of trapped mode. Weisser et al. studied the effect of resonant inclusions inside poroelastic materials [15]. High absorption band was found, which was attributed to resonance of modes through modal analysis.

Void inclusions was also found to be able to improve sound absorption performance. Sharma el al. investigated sound transmission in a soft elastic medium containing voids analytically and numerically [16]. Based on analytical models, the whole medium was treated as a homogenized medium with equivalent material parameters. Broadband sound attenuation was shown to be caused by strong coupling of resonance of voids. The sound propagation properties in soft elastic medium containing voids with a steel backing was further investigated by Sharma et al. [17]. In their research, high sound absorption peaks attributed to Fabry-Pérot resonance was observed. Sharma et al. further investigated sound absorption of an elastic layer simultaneously containing void and hard scatterers [18]. It was found that a broadband high sound absorption was achieved by combining hard and void scatterers in the elastic layer.

In our previous research [19], porous materials with gradient properties are demonstrated to perform better in anechoic chambers with reduced decoration space, compared with the classic wedge design. The proposed uniform-then-gradient flat-wall (UGFW) structure requires a uniform porous material layer in the front, followed by porous materials with gradient properties. In practice, an alternative to making gradient material is replacing the gradient material with multi-layer material. Therefore, the UGFW design can be classified as a special case of the multi-layer, flat-wall (MLFW) design. The idea of MLFW design has been rekindled from the 1980s, e.g. Davern [20] and Dunn and Davern [21], although this idea dated back to 1930s [22]. Recently, Xu et al. conducted real construction of the anechoic chamber based on the optimized MLFW design with different commercially available materials [23-25], which satisfied the ISO standard 3745(2003) [26].

For UGFW design, it is not that easy to obtain the suitable porous materials with desired properties. In this paper, a periodic macro void (PMV) structure is proposed to obtain different properties with a uniform porous material. The equivalent gradient effect is realized through PMV with gradient size. The design of voids with porous materials have been studied both analytically and experimentally, and its performance in sound absorption has also been investigated. Boutin et al. investigated the sound absorption properties of dual porosity material with a simplified model [27]. It was found that introducing dual porosity would enhance absorption properties of porous materials over a wide frequency range. Olny and Boutin proposed a theoretical homogenization model for rigid-frame porous material with double porosities [28]. The macroscopic equivalent parameters were obtained with asymptotic method,

which reveals a strong coupling between the networks in different scales. Boutin and Venega analytically presented equivalent parameters of double porosity materials with elastic frame [29]. With this model, the viscoelastic effect on the equivalent parameters was analyzed. Atalla et al. [30] investigated the effect of macro voids on porous materials, and found that macro perforations could enhance low-frequency absorption of porous materials. Sgard et al. [31] proposed theoretical models for prediction and design of macro voids. Note that the macro voids proposed by Atalla et al. and Sgard et al. were in the normal direction, which is parallel to the sound propagation direction.

In this paper, porous materials with lateral and interior PMV are modelled, and a numerical eigenvalue analysis is conducted with the unit-cell. Based on the calculated eigenvalues and eigenmodes, the equivalent acoustic parameters of PMV porous material are obtained through a homogenization process. The proposed PMV porous material is optimized to realize equivalent gradient absorbers, which provides an alternative to the design of anechoic chambers with improved performance compared with the classic wedge design.

This paper is arranged as follows. Section 2 presents the numerical modelling procedure of PMV porous materials. In Section 3, calculated eigenmodes and equivalent acoustic parameters of the PMV porous material are presented and analyzed. In Section 4, the application of PVM structure in the anechoic chamber is demonstrated. Conclusions are drawn in Section 5.

2 Numerical modelling

2.1 Geometry setting

The geometry of proposed periodic macro void (PMV) porous materials is shown in Fig. 1, as well as the coordinate system, and the wave travels in the direction of x. Note that the term 'macro void' here refers to the portion of space inside the porous material which is full of air. The unit-cell is displayed in the lower part of Fig. 1. The length of the unit-cell in the x direction is d, and the height of the unit-cell is h_0. Inside the unit-cell, the shadowed area represents porous materials, while the blank part represents the macro void. The macro void is circular shape here with the radius of r. The geometric centers of the unit-cell and macro void are O_1 and O_2, respectively. The distance between these two centers are represented with δ_x (positive when O_2 is on the right of O_1 and negative when O_2 is on the left) and δ_y (positive when O_2 is above O_1 and negative when O_2 is below O_1).

The empirical formula proposed by Delany and Bazely [32] is used to model porous materials. With this model, the porous material is treated as an equivalent fluid with frequency-dependent characteristic impedance z_s and wavenumber k_s,

$$\begin{cases} z_s = z_0\left(\left[1+0.057\left(\dfrac{\rho_0 f}{R_f}\right)^{-0.754}\right]-\mathrm{i}\left[0.087\left(\dfrac{\rho_0 f}{R_f}\right)^{-0.732}\right]\right) \\ k_s = k_0\left(\left[1+0.098\left(\dfrac{\rho_0 f}{R_f}\right)^{-0.7}\right]-\mathrm{i}\left[0.189\left(\dfrac{\rho_0 f}{R_f}\right)^{-0.595}\right]\right) \end{cases}, \tag{1}$$

where $z_0 = \rho_0 c_0$ and $k_0 = \omega/c_0$ are the characteristic acoustic impedance and wavenumber in air, respectively; $\mathrm{i} = \sqrt{-1}$, $\omega = 2\pi f$ is angular frequency; f is frequency; ρ_0 is density of air; c_0 is speed of sound in air and R_f is flow resistivity of the porous material. It is suggested that these empirical formulas are valid in the parameter range of $0.01 < \rho_0 f/R_f < 1$. The frequency-dependent speed of sound c_s and density ρ_s for porous materials are calculated as $c_s = \omega/k_s$ and $\rho_s = z_s/c_s$.

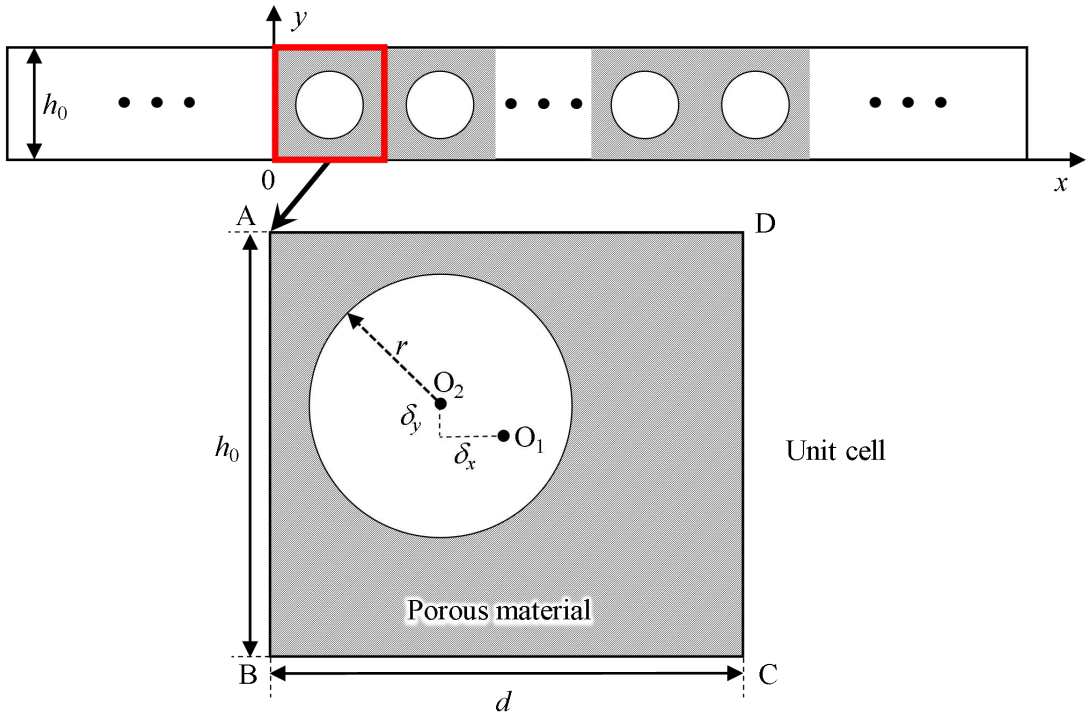

Fig. 1. Geometry of the PMV porous material and its unit-cell.

2.2 Eigenvalue analysis and homogenization

In the literature, different methods have been proposed to deal with sound propagation in materials with inner scatterers, which can be analytical homogenization method [10, 16-18], semi-analytical method based on mode matching [7, 15, 33], numerical method based on finite element (FE) [14] and so on. In this study, a numerical eigenvalue analysis is conducted for the unit-cell, and the equivalent parameters are obtained through a homogenization process with calculated eigenvalues and eigenmodes.

In the first step, the unit-cell is taken out for eigenvalue analysis. The calculation is conducted in the frequency domain, so the time-dependent factor $e^{i\omega t}$ is omitted, and the governing equation for the unit-cell is the linear homogeneous Helmholtz equation

$$\nabla^2 p + k^2 p = 0, \tag{2}$$

where p is the acoustic pressure, k is the wavenumber of the material, being k_0 for air domain and k_s for porous material domain. The particle velocity $\mathbf{v}$ is calculated as

$$\mathbf{v} = -\frac{1}{\mathrm{i}\omega\rho}\nabla p, \tag{3}$$

where ρ is the density of the material, being ρ_0 for air domain and ρ_s for porous material domain.

The continuity of pressure and normal component of particle velocity is applied on the interface between the air domain and the porous material domain, which is expressed as

$$\begin{cases} p_{\text{air}} = p_{\text{porous}} \\ (\mathbf{v}\cdot\mathbf{n})_{\text{air}} = (\mathbf{v}\cdot\mathbf{n})_{\text{porous}} \end{cases}, \tag{4}$$

where $\mathbf{n}$ represents normal vector of the boundary. Rigid wall boundary condition is applied on boundaries AD and BC, which requires the normal component of particle velocity to vanish, and is expressed as

$$\mathbf{v}\cdot\mathbf{n} = 0. \tag{5}$$

On boundaries AB and CD, Floquet-Bloch periodic boundary condition is used [2], which is expressed as

$$\begin{cases} p_{\text{CD}} = \lambda p_{\text{AB}} \\ v_{x\text{CD}} = \lambda v_{x\text{AB}} \end{cases}, \tag{6}$$

where v_x represents the x component of particle velocity, and λ is the eigenvalue to be solved, which corresponds to the Bloch wavenumber k_c with $\lambda = e^{-ik_c d}$.

The eigenvalue analysis is conducted for this unit-cell with the wave finite element (WFE) method [5, 34], which is described in detail in Appendix A. The prototype of the WFE procrdure can be found in the literature dating back to 1970s, when Mead proposed a generalized theory to handle wave propagation in periodic structures [35]. The procedure used in this paper was proposed by Mace et al. in 2005 [34]. A similar procedure was also proposed in the same year by Houillon et al. [36]. These approaches are classified as wave finite element (WFE) method. The WFE method has been successfully applied to investigate wave propagation problems in beams [37, 38], one-dimensional structures [39], plates [40, 41], poroelastic materials [42, 43], periodic structures with complicated unit-cells [44] as well as structural health monitoring [45].

The procedure of the WFE method used in this paper is briefly listed for completeness. The two-dimensional (2D) model of the unit-cell is firstly built in COMSOL Multiphysics® with governing equations and boundary conditions described above. In this model, the unstructured mesh and second-order Lagrange element are used for discritization. After builidng the 2D model, the derived stiffness, damping and mass matrixes are extracted from COMSOL Multiphysics® for further calculation. The eignevalue problem is then formed in MATLAB with the extracted matrixes according to the WFE method described in Appendiex A. Solving the eigenvalue problem with the 'eig' function in MATLAB, which is the embedded eigenvalue solver in MATLAB, the eigenmodes and corresponding eigenvalues are obtained. The eigenvalue λ corresponds to the Bloch wavenumber k_c of the periodic structure with the relationship $\lambda = \mathrm{e}^{-\mathrm{i}k_c d}$, and the first half of the eigenvector is for nodal degree of freedoms (DOFs), which corresponds to the eigenmode shape. Note that the eigenvalue problem is solved at each frequency step, so the frequency-dependent properties are obtained through frequency sweep.

In the second step, a homogenization process is applied to obtain the equivalent acoustic parameters of the PMV porous material. When the homogenization condition of separation of scales in micro and macro descriptions [5, 46] is satisfied, the PMV porous material can be treated as a uniform material with equivalent speed of sound c_c and equivalent density ρ_c. Several analytical homogenization methods have been proposed to obtain the equivalent parameters of materials with inner structures, which can be porous materials with double porosity [28, 29], voids and hard inclusions [10, 16-18] in elastic medium and so on. In this study, a homogenization approach based on the numerical eigenvalue analysis is applied. The Bloch wavenumber k_c is obtained from the eigenvalue λ with

$$k_c = \frac{1}{-\mathrm{i}d}\ln(\lambda). \tag{7}$$

The equivalent speed of sound c_c is defined as the phase velocity of the least decay mode, referred to as the fundamental mode, which is obtained directly from the Bloch wavenumber k_c as

$$c_c = \frac{\omega}{k_c}. \tag{8}$$

The characteristic impedance z_c is defined as the averaged surface impedance on left boundary (AB) or right boundary (CD) of the unit-cell,

$$z_c = \frac{\overline{p}_{\mathrm{AB}}}{\overline{v}_{x\mathrm{AB}}} = \frac{\overline{p}_{\mathrm{CD}}}{\overline{v}_{x\mathrm{CD}}}, \tag{9}$$

which should be the same according to the periodic boundary condition. Note that, the applicability of Eq. (9) is supported by full FE simulation and experiment, which will be shown in the following section. In the parameter range calculated in this study, Eq. (9) is applicable for

different sizes and positions of the macro void. Hence, the equivalent density ρ_c and equivalent bulk modulus κ_c are calculated as

$$\rho_c = \frac{z_c}{c_c},\ \kappa_c = \rho_c c_c^2 . \tag{10}$$

3 Results and analysis

3.1 Eigenmodes and equivalent parameters

In the following analysis, the frequency f is normalized by the height of the unit-cell h_0 and the speed of sound in air c_0, and denoted by a superscript asterisk, as

$$f^* = \frac{f h_0}{c_0} . \tag{11}$$

In this study, the frequency range is chosen as $f^* \leq 0.05$, where the homogenization condition of separation of scales in micro and macro descriptions [5, 46] is satisfied. A calculation example of the eigenmode is presented. The geometric setting is $d = h_0 = 0.02$ m, $r = 0.007$ m, $\delta_x = 0$ and $\delta_y = 0$. In this case, the macro porosity ϕ, which is defined as the ratio of macro void estimate (area for 2D structure and volume for 3D structure) and total estimate, is determined as 38.5%. The calculation frequency is set as $f^* = 0.02$, and the flow resistivity R_f is chosen to be 4000 Pa·s/m^2. The unstructured mesh is used and dispalyed in Fig. 2(a), and pressure field of the fundamental mode is shown in Fig. 2(b).

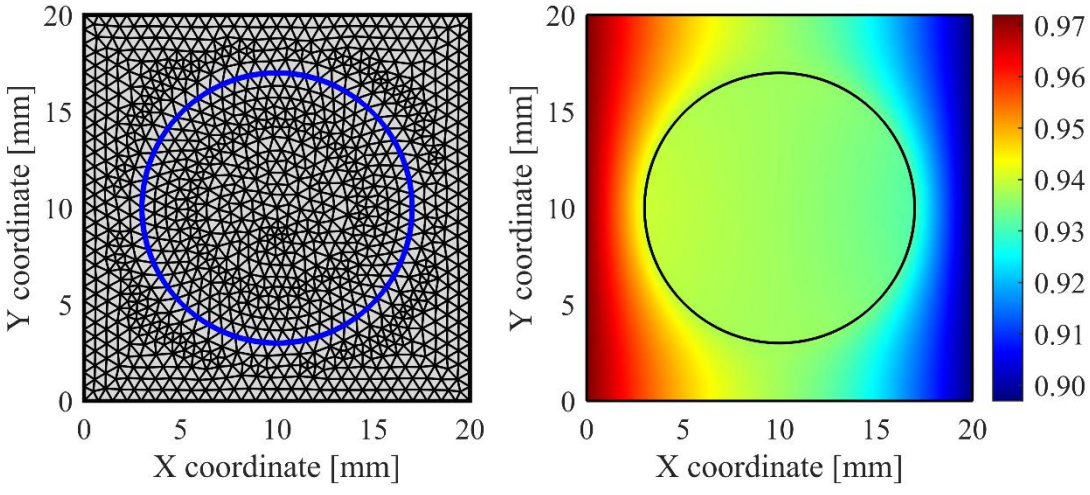

(a) (b)

Fig. 2. Mesh and pressure field (real part) [Pa] of fundamental mode for unit-cell of the PMV porous material at $f^* = 0.02$; (a) mesh; (b) pressure field.

The convergence of calculated Bloch wavenumbers k_c with mesh size S_e is investigated. The mesh size is defined as the maximum element size of the mesh. The case of uniform porous materials without PMV is used for convergence checking as it is a non-trivial task to obtain

analytical eigenvalue of the PMV porous material. A relative error ε_r is defined, to show the convergence of the proposed method, as

$$\varepsilon_r = \left| \left(k_c - k_s \right) / k_s \right|, \tag{12}$$

where k_c is the value calculated by numerical eigenvalue analysis, and k_s is calculated by Eq. (1). The relative error ε_r of calculated wavenumbers for the fundamental mode at three different frequencies are displayed in Fig. 3. It is found that the wavenumbers obey a convenience rate of S_e^4 for all three frequencies. Meanwhile, smaller mesh size is needed for higher frequency to achieve the same accuracy as lower frequency.

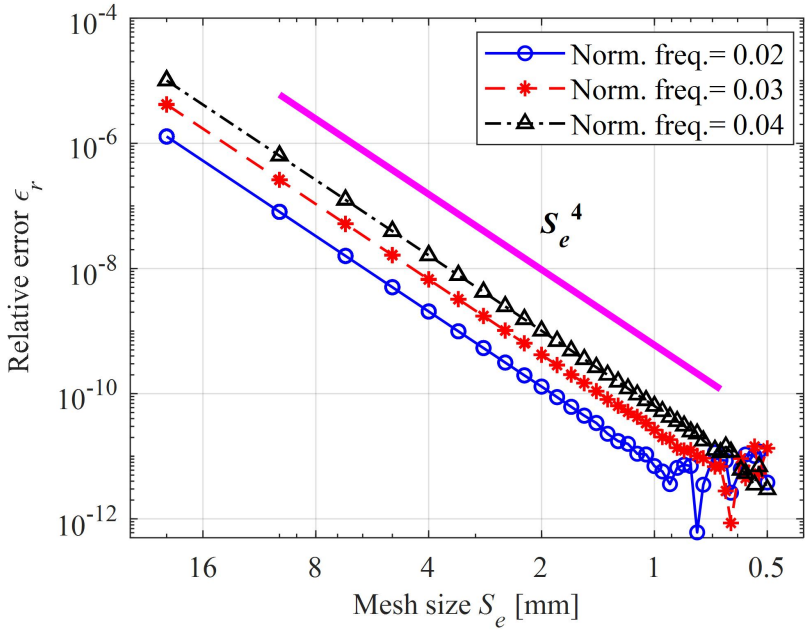

Fig. 3. Convergence of calculated wavenumbers with mesh size S_e.

In the following analysis, the acoustic quantities are normalized by a set of basic physical parameters: the height of the unit-cell h_0, speed of sound in air c_0, and air density ρ_0. The normalized physical variables are denoted by a superscript asterisk, as shown below

$$\rho_c^* = \frac{\rho_c}{\rho_0}, \quad c_c^* = \frac{c_c}{c_0}, \quad z_c^* = \frac{z_c}{\rho_0 c_0}, \quad \kappa_c^* = \frac{\kappa_c}{\rho_0 c_0^2}. \tag{13}$$

Applying the homogenization process and normalization of physical variables, the normalized equivalent acoustic parameters are obtained through frequency sweep, as the characteristics of porous materials are frequency-dependent.

The equivalent density and bulk modulus of the PMV porous material described above are displayed in Fig. 4, together with the results of the porous material without PMV. It is found that, with PMV, both real and imaginary parts of equivalent density become smaller. The decreased imaginary density means decreased viscous damping, which is a natural result of decreased amount of sound absorption material. The decreased real density (mass) represents decreased

tortuosity, which is reasonable because the tortuosity of the void domain is 1 (smallest). For equivalent bulk modulus of the PMV porous material, its real part becomes larger while its imaginary part becomes smaller, and both real and imaginary parts become closer to that of air. The increased real part of bulk modulus means increased stiffness, while the decreased imaginary part of bulk modulus represents decreased thermal conduction effect.

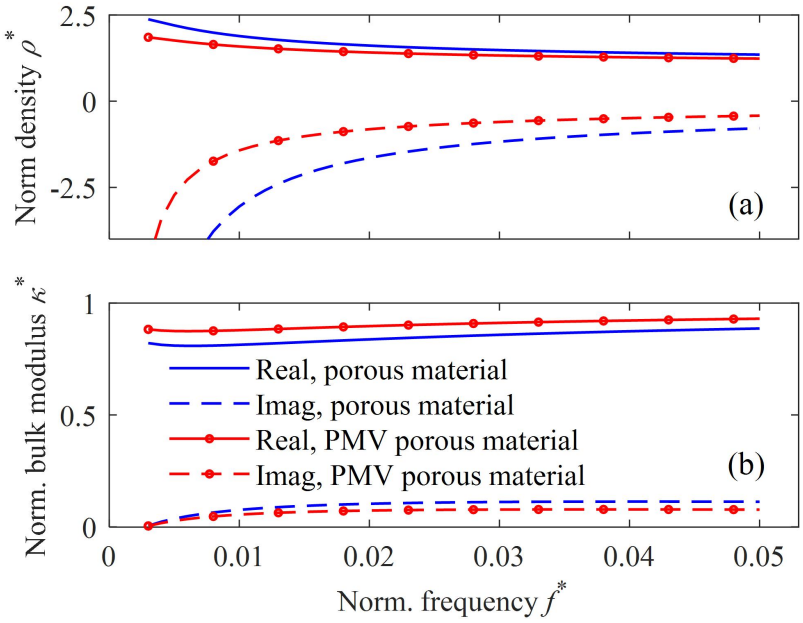

Fig. 4. Normalized equivalent density and bulk modulus of the PMV porous material with R_f = 4000 Pa·s/m^2 and macro porosity ϕ = 38.5%.

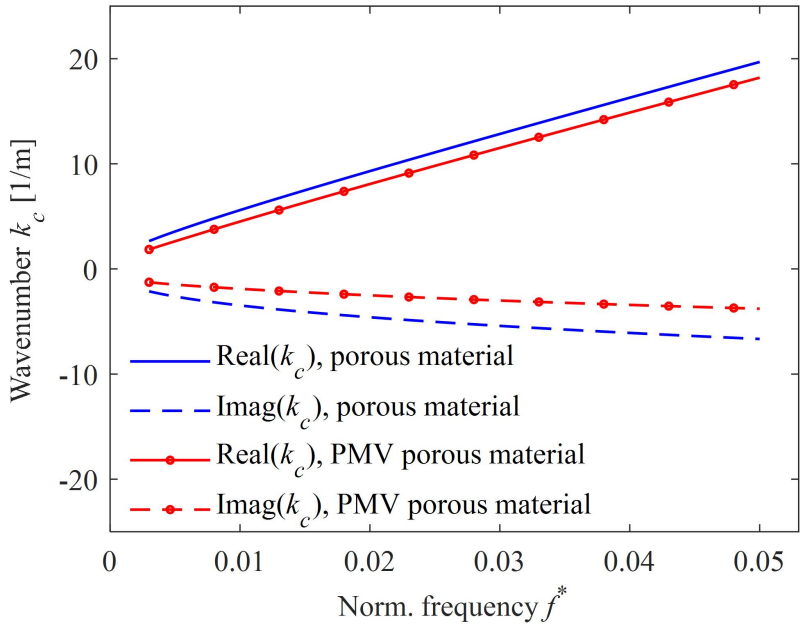

Fig. 5. Dispersion curve for fundamental mode of the PMV porous material with R_f = 4000 Pa·s/m^2 and macro porosity ϕ = 38.5%.

The PMV porous material can be regarded as a composite of normal porous material and air, whose equivalent parameters are between those of air and those of normal porous materials. As a result of decreased mass and increased bulk modulus compared with normal porous materials, the increased equivalent speed of sound is obtained, which is shown in the dispersion curve in Fig. 5 as decreased real part of wavenumbers. The decreased imaginary part of wavenumbers can be explained by the decreased viscous damping and thermal conduction effect.

3.2 Validation for equivalent acoustic parameters

Finite structure simulations and experiments are conducted to validate the calculated results of the equivalent density and bulk modulus for PMV porous materials.

PMV porous materials with 5 unit-cells are taken out for analysis. The 5-unit structure is simulated by commercial FE software (COMSOL Multiphysics®) with the method described in reference [5], which is provided in the Appendix B for completeness. The result of 5-unit simulation is shown in Fig. 6, which matches well with the result from WFE prediction.

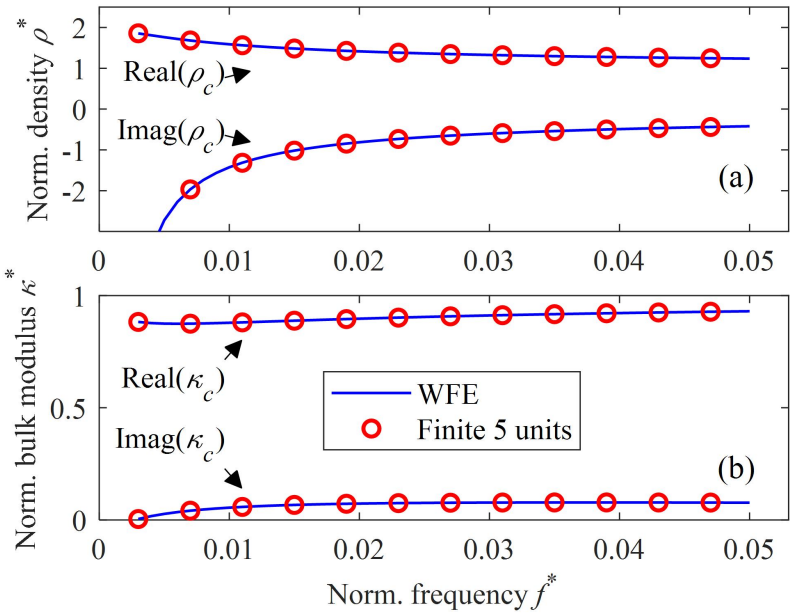

Fig. 6. Normalized Equivalent density and bulk modulus of the PMV porous material validated by finite structure simulation with 5 units.

In addition, an experiment is conducted to validate the calculated equivalent parameters with the sample containing 5 units. The test sample of the PMV porous material is displayed in Fig. 7. It is made of polyester foam with the density of 50 kg/m^3. The size of the sample is 100 × 100 × 100 mm. The macro voids are in the y direction, while the sound comes from x direction. The PMVs are made by drilling holes in y direction with a foam hole opener. In other words, the PMVs are in the lateral direction. There are 5 units in both x and z directions, and the size of the unit-cell is 0.02 m. The macro voids are in circular shape, with the radius of 0.007 m, so the macro porosity is ϕ = 38.5%.

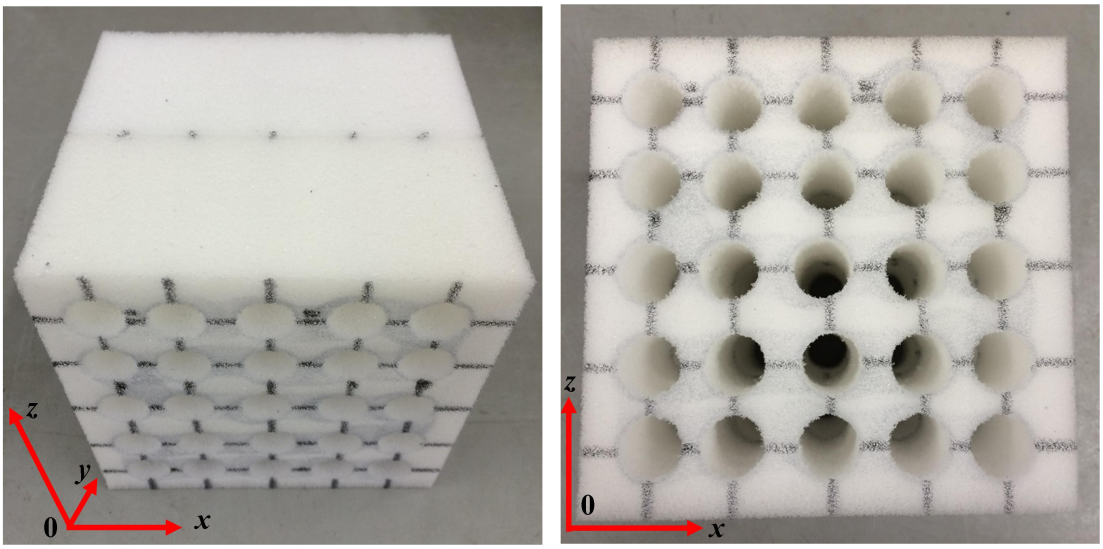

(a) (b)

Fig. 7. Test sample of the PMV porous material, with macro porosity ϕ = 38.5%; (a) 3D view; (b) cross-sectional view.

The equivalent density and bulk modulus can be obtained through the two-cavity method proposed by Utsuno et al. [47] in an impedance tube [48]. The tested equivalent density and bulk modulus of the uniform foam sample without PMV are displayed in Fig. 8 (solid and dash lines for real and imaginary parts, respectively). The equivalent density and bulk modulus are then used to conduct the eigenvalue analysis and homogenization to obtain equivalent parameters of PMV foam, which are shown in Fig. 8 (solid star and dash star lines for real and imaginary parts, respectively). On the other hand, the equivalent density and bulk modulus of the PMV foam are obtained directly from experiment through the two-cavity method, which are also depicted in Fig. 8 (circular and triangular points for real and imaginary parts, respectively). It is found that with PMV, both real and imaginary parts of equivalent density of the porous material become smaller, which is in accordance with results in Section 3.1 from Delany's model. In addition, increased real part and decreased imaginary part of equivalent bulk modulus with PMV are observed, which also validates the results with Delany's empirical formula. The experimental results of equivalent parameters of PMV porous materials generally match the results from prediction, which further validates the calculation method.

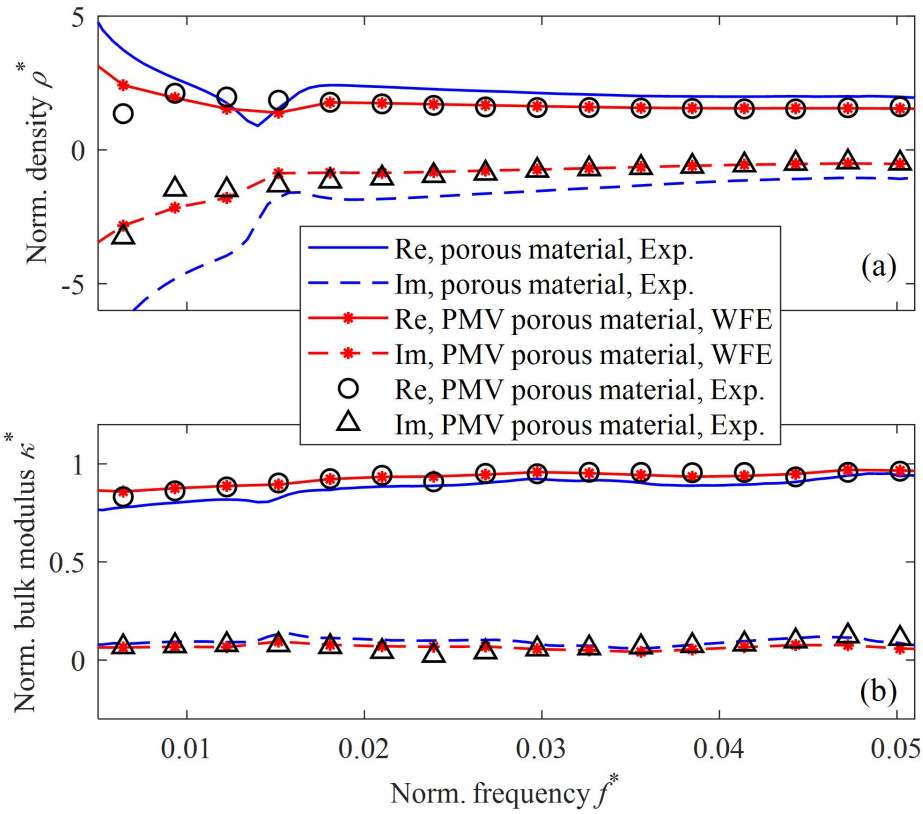

Fig. 8. Normalized equivalent density and bulk modulus of the PMV porous material validated by experiments with macro porosity ϕ = 38.5%.

3.3 Geometric parameter analysis

The effects of three geometric parameters of PMV on porous materials are investigated, which are the void shape, void position and macro porosity.

The equivalent density and bulk modulus of PMV porous materials with four kinds of void shapes are calculated, which are square, hexagon, octagon, and circle. The center of the PMV is set to coincide with center of the unit-cell (δ_x=0, δ_y=0). The calculated results of these four void shapes with the same macro porosity (ϕ = 38.5%) are displayed in Fig. 9. It is found that both equivalent density and bulk modulus are independent of the void shape in the calculated frequency range, as long as the macro porosity is kept unchanged. Similar result was reported by Groby et al. with hard inclusions [9].

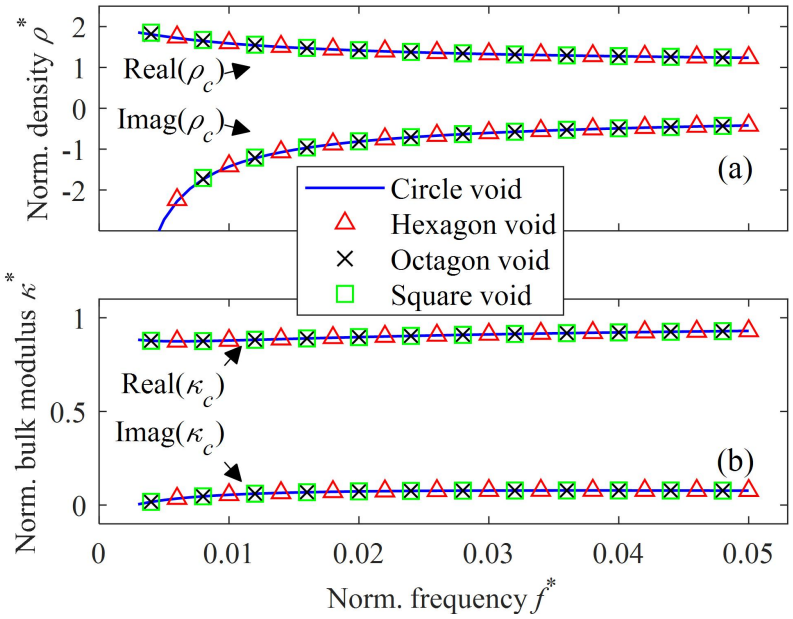

Fig. 9. Normalized equivalent density and bulk modulus of PMV porous materials with different macro void shapes.

The effect of void center position on the equivalent density and bulk modulus are studied, with the change of geometric parameters N_{px} and N_{py}, which are defined as

$$N_{px} = \frac{\delta_x}{d}, N_{py} = \frac{\delta_y}{h_0}. \tag{14}$$

The effect of N_{px} and N_{py} on the equivalent density and bulk modulus at fixed frequency $f^* = 0.02$ are displayed in Fig. 10 (a-d), respectively. It is shown that the position of the void center has little effect on the equivalent acoustic parameters of PMV porous materials.

The effect of macro porosity ϕ on equivalent acoustic parameters of PMV porous materials are studied, and the results are shown in Fig. 11. It is found that the dependence of equivalent density and bulk modulus with respect to macro porosity is generally linear, which indicates that the equivalent acoustic parameters of PMV porous materials are almost linear combination of uniform porous materials and air.

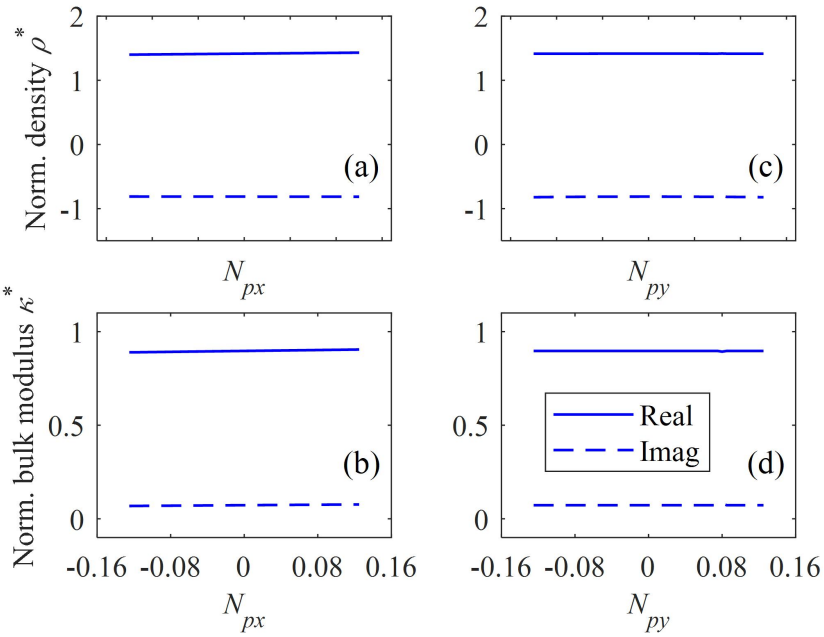

Fig. 10. Normalized equivalent density and bulk modulus of PMV porous materials with change of void center position at frequency $f^* = 0.02$; (a) density, void center change in x direction; (b) density, void center change in y direction; (c) bulk modulus, void center change in x direction; (d) bulk modulus, void center change in y direction.

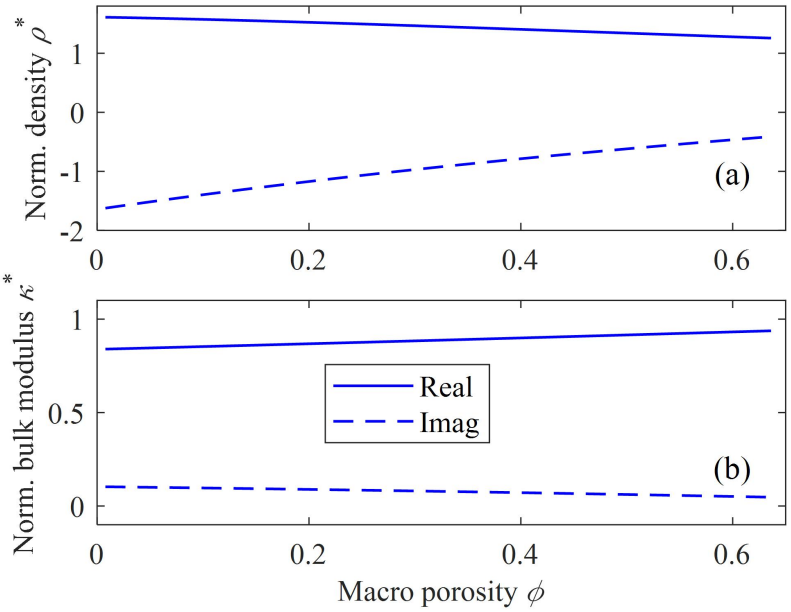

Fig. 11. Normalized equivalent density and bulk modulus of PMV porous materials with change of macro porosity ϕ, at frequency $f^* = 0.02$; (a) equivalent density; (b) equivalent bulk modulus.

3.4 Gradient macro porosity for sound absorption

The gradient PMV porous materials have the potential to enhance sound absorption performance of uniform porous materials. An experimental example in an impedance tube for

rigid-backed sound absorption coefficient is provided. The foam tested in Section 3.2 is used to make several samples of PMV porous materials with different macro porosities.

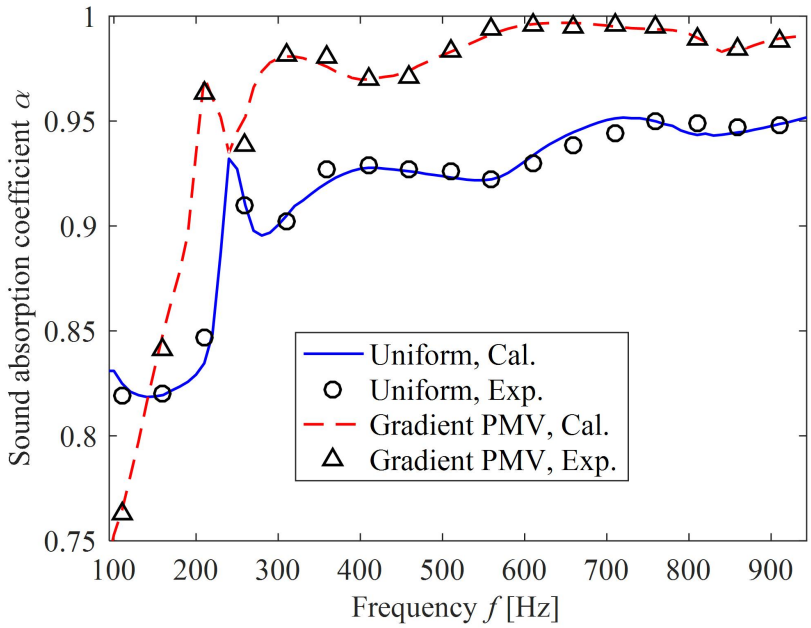

Fig. 12. Experimental results of sound absorption coefficient for uniform and gradient PMV porous materials with length of 0.4 m.

The total length of the sound absorption material is chosen to be 0.4 m. Therefore, the absorption part is divided into 4 layers, and each layer has a length of 0.1 m, which is the length of one foam sample. The sound absorption coefficient of different combinations of PMV porous materials are tested and compared with the uniform foam. The best combination of macro porosity distribution, obtained from the testing results, is 50.3%, 12.6%, 7.1% and 0% from the surface of the absorption part to the rigid end. The tested best sound absorption coefficient is displayed in Fig. 12, together with the tested result for uniform foam of the same length. It is shown that the normal incidence sound absorption coefficient is greatly enhanced with the gradient PMV structure. Besides, the experimental result matches well with predictions, which further validates the proposed simulation method.

4 Application for anechoic chamber

In this section, the gradient PMV structure is optimized for the application of anechoic chambers. Its performance is compared with the classic wedge design [19]. In this section, the three-dimensional (3D) void design is proposed, which is displayed in Fig. 13. The unit-cell is set to be cubic with the length of d, and the PMV is also set as cubic shape with the length of d_1. The two geometrical centers are located at the same point. For manufacturing of such kind of structure, a three-step procedure is proposed. In the first step, a layer is cut from the uniform porous material. In the second step, macro voids are made with the remaining porous material. In

the final step, the layer cut from the porous material is glued to the voided porous material. Some performance change of the PMV structure may be introduced by the manufacturing procedure, which will be investigated in the further study and not discussed in this paper.

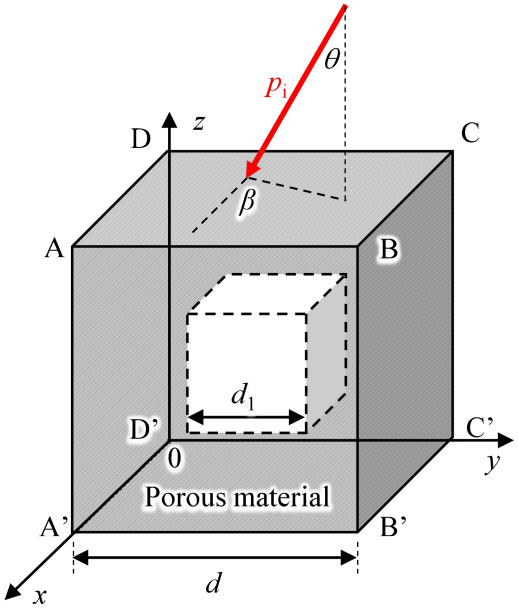

Fig. 13. Geometry for unit-cell of three-dimensional (3D) PMV design.

4.1 Oblique incidence modelling for 3D unit

To simulate its acoustic performance in anechoic chambers, the effect of oblique incidence is considered. The equivalent density and bulk modulus of the 3D PMV porous material at oblique incidence are obtained by conducting the eigenvalue analysis with the WFE method and a homogenization process described as follows.

As shown in Fig. 13, the oblique incident sound p_i comes from the top, with the incident angle of θ and β, which are the elevation angle and azimuth angle, respectively. Boundaries DCC′D′ and ABB′A′ are applied with a constant phase angle difference of $e^{ik_x d}$ with $k_x = k_0 \sin\theta\cos\beta$, and boundaries ADD′A′ and BCC′B′ are applied with a constant phase angle difference of $e^{ik_y d}$ with $k_y = k_0 \sin\theta\sin\beta$. Boundaries ABCD and A′B′C′D′ are applied with Floquet-Bloch periodic boundary condition as

$$\begin{cases} p_B = \lambda p_T \\ v_{zB} = \lambda v_{zT} \end{cases}, \tag{15}$$

where p_B and p_T are the acoustic pressures on the bottom (A′B′C′D′) and top (ABCD) boundaries, respectively; v_{zB} and v_{zT} are the z component of acoustic particle velocity on the bottom (A′B′C′D′) and top (ABCD) boundaries, respectively; and λ is the eigenvalue to be determined, which corresponds to the Bloch wavenumber k_c through the following relationship

$$\lambda = \mathrm{e}^{\mathrm{i}k_c \cos(\theta')d}, \tag{16}$$

where θ' is the refraction angle inside the PMV porous material, which is defined as

$$\theta' = \arcsin\left(\frac{k_0}{k_c}\sin\theta\right). \tag{17}$$

Combining the above periodic boundary condition with the WFE formulation, the eigenvalue problem of the oblique incidence in obtained. Solving this eigenvalue problem, and conducting homogenization on the fundamental mode, the equivalent acoustic parameters at oblique incidence are obtained.

The equivalent speed of sound c_c is obtained from the Bloch wavenumber k_c, as $c_c = \omega/k_c$ .The equivalent characteristic impedance z_c is defined as $z_c = z_{\mathbf{n}s} \cdot \cos\theta'$, where $z_{\mathbf{n}s}$ is the normal surface impedance on boundary ABCD or A′B′C′D′ , which is defined as

$$z_{\mathbf{n}s} = \frac{\overline{p}_{\mathrm{ABCD}}}{\overline{v}_{z\mathrm{ABCD}}} = \frac{\overline{p}_{\mathrm{A'B'C'D'}}}{\overline{v}_{z\mathrm{A'B'C'D'}}}. \tag{18}$$

The example of a 3D PMV porous material with flow resistivity R_f = 4000 Pa·s/m^2 is calculated and the equivalent density and bulk modulus at two incident angles are shown in Fig. 14. In this example, the length of the unit-cell is chosen as d = 0.02 m, and the macro porosity ϕ is set as 38.5%, which is the same as the example of 2D unit. It is found that, the equivalent parameters are nearly independent from incident angle, which means that the equivalent acoustic parameters obtained from normal incidence can be used to predict its performance at oblique incidence. This result further supports the homogenization process, because the 3D PMV porous material performs like an isotropic uniform material.

The independence of equivalent parameters on incident angles is double-checked by sound absorption coefficient calculation with COMSOL Multiphysics®. A layer of PMV porous material with thickness of 0.1m (5 units) and macro porosity of ϕ = 38.5% is used, which is referred to as the sample PMV. The sound absorption coefficients (α) of the rigid-backed sample PMV at different incident angles are calculated with the following two methods. The first method is using direct FE calculation with the exact geometry of 5 units with PMVs. The second method is treating the sample PMV as 0.1 m uniform material with equivalent parameters obtained from normal incidence case (θ = 0°). The calculated α at two incident angles (θ = 45° and 75°) are depicted in Fig. 15. It is shown that α calculated by the two methods matches well with each other for both 45° and 75° incidence, which indicates that the equivalent parameters of PMV porous materials are nearly independent from the incident angle.

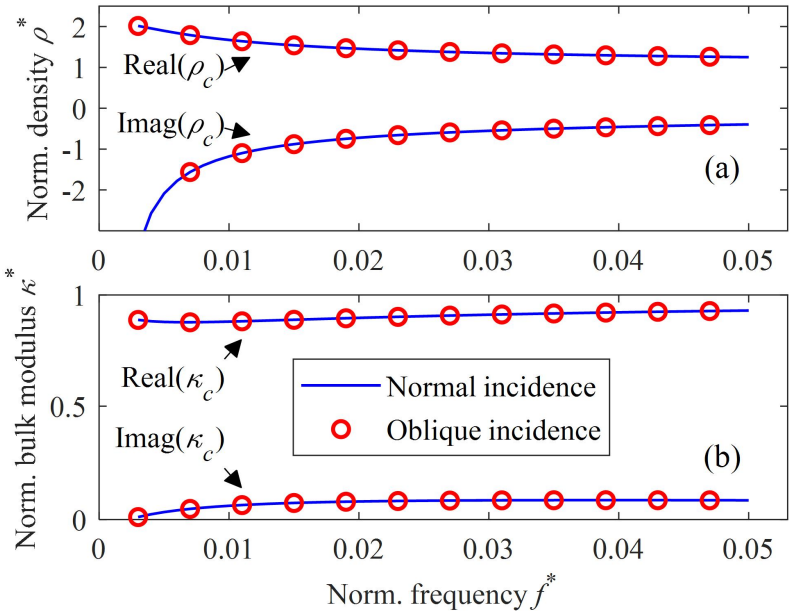

Fig. 14. Normalized equivalent density and bulk modulus of the 3D PMV porous material at different incident angles; line: $\theta = 0°$, $\beta = 0°$, circle marker: $\theta = 30°$, $\beta = 60°$.

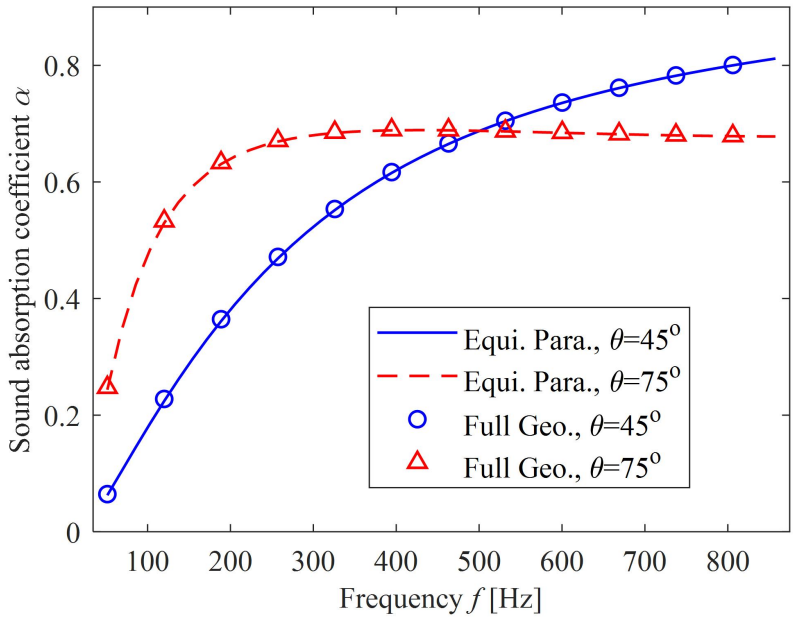

Fig. 15. Oblique incidence sound absorption coefficient α of PMV absorbers with thickness of 0.1 m.

4.2 Gradient PMV optimization for anechoic chambers

Based on the obtained equivalent acoustic parameters, the performance of the gradient PMV porous materials in anechoic chambers is simulated with the modified complex source image (CSI) model [19], which is a modification of the CSI model [49, 50]. With a fixed thickness D, fixed cut-off frequency f_{cutoff} and a fixed flow resistivity R_f (input parameters), the macro porosity

distribution (output parameters) is directly optimized based on its chamber performance. The simulated chamber is 9 m × 8 m ×7 m without considering the decoration thickness, which is the same as that in reference [19]. The point source with unit amplitude is put at the center of the chamber, and the first testing line ranges from the center to one of the eight vertices. The second testing line is from the center of the chamber to the center of the closest wall.

The objective function is set to minimize the average deviation from the inverse square law for the first testing line, and the optimization is conducted with the sequential quadratic programming (SQP) algorithm in MATLAB.

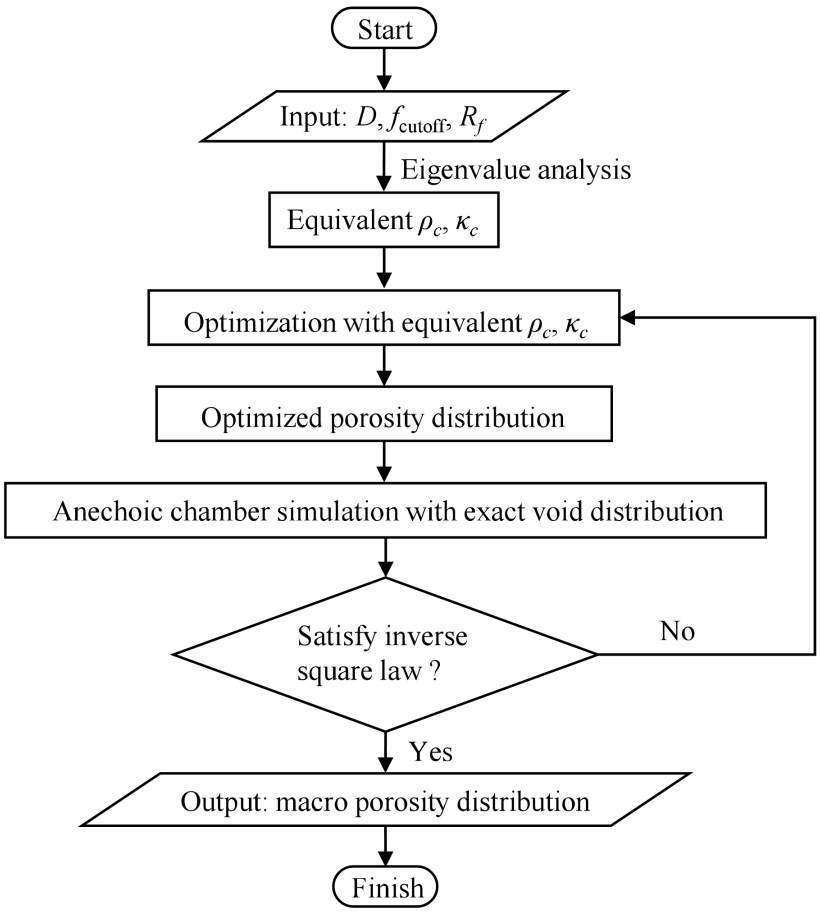

Fig. 16. Anechoic chamber optimization procedure with gradient PMV structure.

Once the optimized porosity distribution is obtained, its performance in anechoic chambers are simulated with exact PMV structures, and double-checked with the inverse square law [26]. If the chamber simulation results satisfy the inverse square law within 1.5 dB deviation, the optimization is completed; otherwise, a new optimization should be conducted until the required results are obtained. The above-mentioned optimization procedure is represented as a flow chart in Fig. 16.

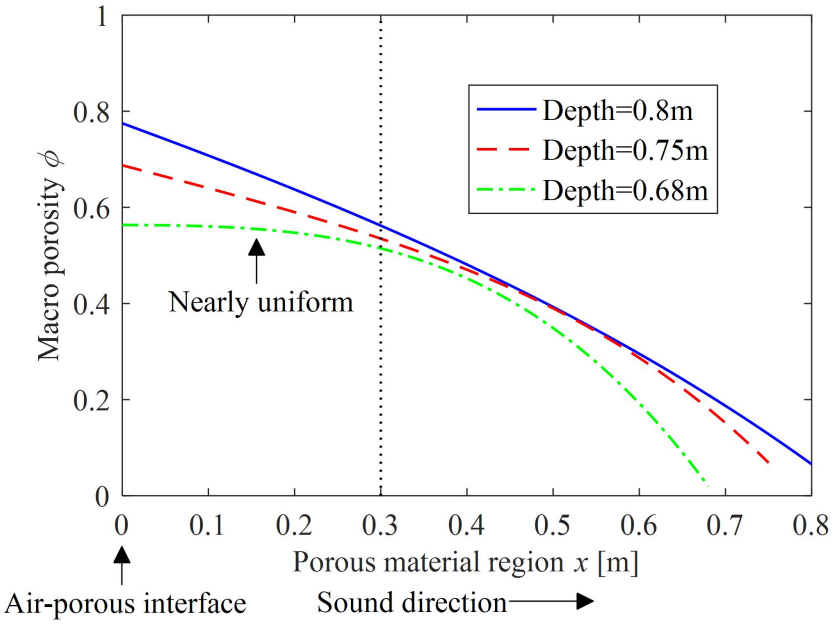

Fig. 17. Optimized macro porosity distribution with different thicknesses (D) for the anechoic chamber, R_f = 5960 Pa·s/m^2, f_{cutoff} = 100 Hz.

The calculation results of optimized macro porosity distribution with different thicknesses are displayed in Fig. 17. In this figure, the horizontal axis represents the direction where sound comes inside the porous material region, and the air-porous interface is chosen as the origin. The flow resistivity R_f is chosen as 5960 Pa·s/m^2, and the cut-off frequency is set to be f_{cutoff} = 100 Hz, which is kept the same as that in reference [19]. It is found that with smaller fixed thickness, the macro porosity distribution displays higher order characteristics with respect to the thickness direction. For the fixed thickness of D = 0.68 m, a nearly uniform porosity is obtained in the front part (x < 0.3 m), which is in accordance with the UGFW design [19]. Therefore, the PMV structure proposed in this paper provides an alternative to realize such design with uniform porous materials.

4.3 Anechoic chamber simulation result

The performance of the gradient PMV design and the wedge design is compared with flow resistivity set as R_f =5960 Pa·s/m^2. The gradient PMV design with thickness D = 0.8 m is firstly picked up to compare with the optimized wedge design with total thickness of D = 0.8 m [19]. The optimized macro porosity distribution of the gradient PMV design with thickness D = 0.8 m is shown in Fig. 17 (solid line).

The sound pressure level (SPL) decaying curves of the optimized wedge and gradient PMV design with D = 0.8 m are displayed in Fig. 18 (a) and (b) respectively for the first testing line and second testing line. For the first testing line, the gradient PMV design satisfies the inverse square law within the 1.5 dB deviation along the testing line, which meats the requirement of the 75% condition [19, 25], while the wedge design violates the 1.5 dB deviation from the inverse

square law before 75% of the testing line. For the second testing line, both wedge design and gradient PMV design satisfy the inverse square law within the 1.5 dB deviation.

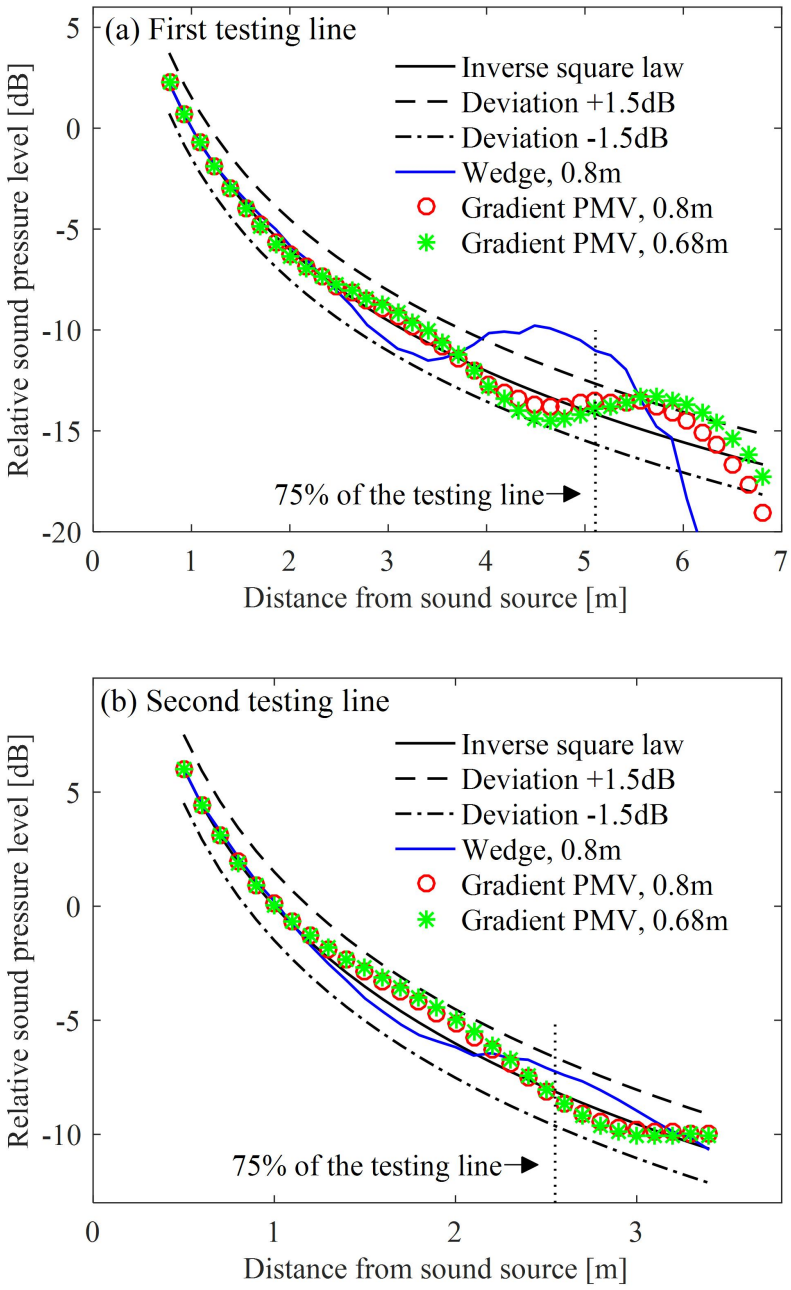

Fig. 18. SPL decaying curves for optimized wedge design with D = 0.8 m and gradient PMV design with thickness D = 0.8 m and 0.68 m at frequency f =100 Hz; (a) for the first testing line; (b) for the second testing line.

The chamber performance of the two designs with same thickness is quantified with average deviation of SPL from the inverse square law ($\mathrm{SPL_{ad}}$) within 75% of the first testing line, which is defined as

$$\mathrm{SPL_{ad}} = \frac{1}{N_{\mathrm{point}}} \sum_{\text{within } 75\%} \left| \mathrm{SPL_{design}} - \mathrm{SPL_{ISL}} \right|, \tag{19}$$

where SPL_{design} and SPL_{ISL} are the calculated SPL along the first testing line, respectively, for different designs and inverse square law; N_{point} is the number of spatial points used in the SPL decay calculation within 75% of the first testing line. It is found that, with the same thickness D = 0.8 m, the SPL_{ad} of the optimized wedge design is 1.10 dB, while the SPL_{ad} of the gradient PMV design is 0.28 dB. In this case, the performance of the gradient PMV design is much better than the wedge design.

The gradient PMV porous materials with different thicknesses are simulated in the anechoic chamber and the minimum thickness that meats the inverse square law within 1.5dB deviation is obtained. With the flow resistivity of 5960 Pa·s/m^2, cut-off frequency of 100Hz and the chamber size of 9 m × 8 m ×7 m, the required minimum thickness for the gradient PMV design is 0.68 m, and the optimized macro-porosity distribution is shown in Fig. 17 with dash dot line. The SPL decaying curves of the optimized gradient PMV design with D = 0.68 m are displayed in Fig. 18 (a) and (b) with star points, respectively, for the first testing line and the second testing line. It is found that, for the first testing line, the gradient PMV design with D = 0.68 m have more space which satisfies the inverse square law within the 1.5 dB deviation, than the wedge design with D = 0.8 m. In addition, gradient PMV design with D = 0.68 m satisfies the requirement of the 75% condition at designed cut-off frequency of 100 Hz, while the wedge design does not. For the second testing line, the gradient PMV design with D = 0.68 m satisfies the inverse square law within the 1.5dB deviation.

The performance of gradient PMV design with reduced thickness is quantified with SPL_{ad} as defined previously. The SPL_{ad} of gradient PMV with thickness D = 0.68 m is 0.43 dB, which is still better than the wedge design (1.10 dB), although the performance is a little bit worse than gradient PMV with thickness D = 0.8 m (0.28 dB). Therefore, the optimized gradient PMV design can achieve better performance than the classic wedge design with the same thickness D = 0.8 m. Moreover, the thickness of gradient PMV design can be reduced up to 15% (D = 0.68 m) while keeping better performance than the wedge design.

In addition to the thickness, the mass of porous materials used for different designs is also investigated. With mass of wedge design as a reference (which is defined as 1), the masses of gradient PMV design are 1.08 and 0.97, respectively, for D = 0.8 m and D = 0.68 m, which are nearly the same as wedge design.

To further analyze the sound absorption effects of the gradient PMV structure, the normalized surface impedance of the gradient PMV structure with thickness D = 0.68 m at different incident angles is presented in Fig. 19, together with the surface impedance of the optimized wedge design. In addition, the required normal surface impedance for perfect match is also depicted in Fig. 19 (solid line with triangle markers). It is found that the gradient PMV structure matches with the required impedance better, when the incident angle is around 45°. It

indicates that such better impedance match contributes to the better performance of the gradient PMV structure in the anechoic chamber simulation, where oblique incidence at around 45° instead of normal incidence is determinate.

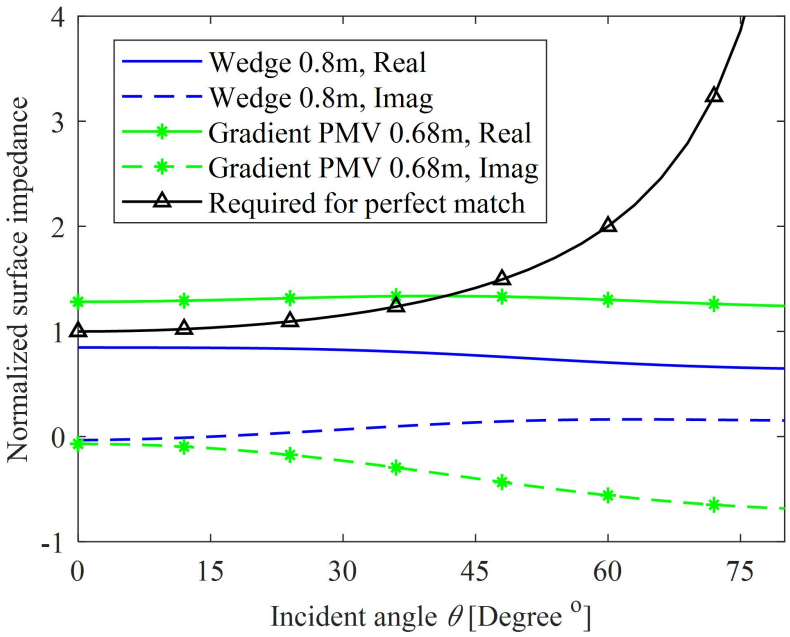

Fig. 19. Normalized surface impedance of optimized wedge design with thickness D = 0.8 m and gradient PMV design with thickness D = 0.68 m, for different incident angles at frequency f = 100 Hz.

5 Conclusions

In this paper, a periodic macro void (PMV) design of porous materials is proposed, through which different acoustic properties can be obtained with uniform porous materials. The equivalent density and bulk modulus of PMV porous materials are obtained through a homogenization process based on the wave finite element (WFE) method. These equivalent acoustic parameters are validated by the finite-unit's simulation and experiment.

The effects of geometric parameters on equivalent acoustic parameters of PMV porous materials are analyzed. It is found that the equivalent density and bulk modulus are independent of the void shape and void position, as long as the macro-porosity is kept unchanged. In the frequency range of interest, the equivalent acoustic parameters of PMV porous materials are between that of normal porous materials and air. The PMV design can be used to realize gradient design of porous materials, which is shown experimentally to have the potential of enhancing sound absorption properties of uniform porous materials.

The three-dimensional (3D) PMV structure was proposed and analyzed under the oblique incidence condition. It is found that the equivalent density and bulk modulus of 3D PMV porous materials are independent of incident angles. Therefore, the gradient PMV design of porous

materials is used to optimize the anechoic chamber performance, and an optimization procedure is provided. For a fixed chamber size of 9 m × 8 m × 7 m, fixed cut-off frequency of 100Hz, the optimized macro porosity distributions of gradient PMV structure with different thicknesses are obtained. The chamber performance for gradient PMV design of porous materials are presented with thickness D = 0.8 m and 0.68 m, which are compared with the optimized wedge design. It is found that the optimized gradient PMV design can achieve better performance than the classic wedge design with the same thickness of 0.8 m. Moreover, the thickness of gradient PMV design can be reduced up to 15% (0.68 m) while keeping better performance than the wedge design.

To summarize, the proposed PMV design of porous materials provides an alternative to realize the gradient sound absorbers, which is shown to have the potential in enhancing sound absorption properties of porous materials and perform better than the classic wedge design in anechoic chambers.

Acknowledgment

Part of the work was accomplished when the first author was a PhD student and Post-Doctoral Fellow in The University of Hong Kong. This project is supported by National Natural Science Foundation of China (Grant No. 51775467).

References

[1] E.D. Nobrega, F. Gautier, A. Pelat, J.M.C. Dos Santos, Vibration band gaps for elastic metamaterial rods using wave finite element method, Mech. Syst. Signal Proc., 79 (2016) 192-202.

[2] C.E. Bradley, Time-harmonic acoustic Bloch wave-propagation in periodic wave-guides. Part 1. Theory, J. Acoust. Soc. Am., 96 (1994) 1844-1853.

[3] D. Bai, J.B. Keller, Sound waves in a periodic medium containing rigid spheres, J. Acoust. Soc. Am., 82 (1987) 1436-1441.

[4] A.A. Krokhin, J. Arriaga, L.N. Gumen, Speed of sound in periodic elastic composites, Phys. Rev. Lett., 91 (2003).

[5] C. Jiang, L. Huang, Characterization of low-frequency acoustic wave propagation through a periodic corrugated waveguide, J. Sound Vib., 418 (2018) 79-99.

[6] J.P. Groby, A. Wirgin, L. De Ryck, W. Lauriks, R.P. Gilbert, Y.S. Xu, Acoustic response of a rigid-frame porous medium plate with a periodic set of inclusions, J. Acoust. Soc. Am., 126 (2009) 685-693.

[7] J.P. Groby, O. Dazel, A. Duclos, L. Boeckx, L. Kelders, Enhancing the absorption coefficient of a backed rigid frame porous layer by embedding circular periodic inclusions, J. Acoust. Soc. Am., 130 (2011) 3771-3780.

[8] J.P. Groby, A. Duclos, O. Dazel, L. Boeckx, W. Lauriks, Absorption of a rigid frame porous layer with periodic circular inclusions backed by a periodic grating, J. Acoust. Soc. Am., 129 (2011) 3035-3046.

[9] J.P. Groby, C. Lagarrigue, B. Brouard, O. Dazel, V. Tournat, B. Nennig, Using simple shape three-dimensional rigid inclusions to enhance porous layer absorption, J. Acoust. Soc. Am., 136 (2014) 1139-1148.

[10] G.S. Sharma, A. Skvortsov, I. MacGillivray, N. Kessissoglou, Acoustic performance of periodic steel cylinders embedded in a viscoelastic medium, J. Sound Vib., 443 (2019) 652-665.

[11] C. Boutin, Acoustics of porous media with inner resonators, J. Acoust. Soc. Am., 134 (2013) 4717-4729.

[12] C. Lagarrigue, J.P. Groby, V. Tournat, O. Dazel, O. Umnova, Absorption of sound by porous layers with embedded periodic arrays of resonant inclusions, J. Acoust. Soc. Am., 134 (2013) 4670-4680.

[13] C. Boutin, F.X. Becot, Theory and experiments on poro-acoustics with inner resonators, Wave Motion, 54 (2015) 76-99.

[14] J.P. Groby, C. Lagarrigue, B. Brouard, O. Dazel, V. Tournat, B. Nennig, Enhancing the absorption properties of acoustic porous plates by periodically embedding Helmholtz resonators, J. Acoust. Soc. Am., 137 (2015) 273-280.

[15] T. Weisser, J.P. Groby, O. Dazel, F. Gaultier, E. Deckers, S. Futatsugi, L. Monteiro, Acoustic behavior of a rigidly backed poroelastic layer with periodic resonant inclusions by a multiple scattering approach, J. Acoust. Soc. Am., 139 (2016) 617-629.

[16] G.S. Sharma, A. Skvortsov, I. MacGillivray, N. Kessissoglou, Sound transmission through a periodically voided soft elastic medium submerged in water, Wave Motion, 70 (2017) 101-112.

[17] G.S. Sharma, A. Skvortsov, I. MacGillivray, N. Kessissoglou, Acoustic performance of gratings of cylindrical voids in a soft elastic medium with a steel backing, J. Acoust. Soc. Am., 141 (2017) 4694-4704.

[18] G.S. Sharma, A. Skvortsov, I. MacGillivray, N. Kessissoglou, Sound absorption by rubber coatings with periodic voids and hard inclusions, Appl. Acoust., 143 (2019) 200-210.

[19] C. Jiang, S. Zhang, L. Huang, On the acoustic wedge design and simulation of anechoic chamber, J. Sound Vib., 381 (2016) 139-155.

[20] W.A. Davern, Flat-walled graded density anechoic lining, Tenth International Congress on Acoustics, Sydney, Australia, 1980.

[21] I.P. Dunn, W.A. Davern, Calculation of acoustic impedance of multi-layer absorbers, Appl. Acoust., 19 (1986) 321-334.

[22] E.H. Bedell, Some data on a room designed for free field measurements, J. Acoust. Soc. Am., 8 (1936) 118-125.

[23] J. Xu, J. Nannariello, F.R. Fricke, Optimising flat-walled multi-layered anechoic linings using evolutionary algorithms, Appl. Acoust., 65 (2004) 1009-1026.

[24] J. Xu, J.M. Buchholz, F.R. Fricke, Application of multi-layered polyurethane foams for flat-walled anechoic linings, Appl. Acoust., 67 (2006) 476-485.

[25] J. Xu, J.M. Buchholz, F.R. Fricke, Flat-walled multilayered anechoic linings: Optimization and application, J. Acoust. Soc. Am., 118 (2005) 3104-3109.

[26] ISO, ISO 3745 Acoustics — Determination of sound power levels of noise sources using sound pressure — Precision methods for anechoic and hemi-anechoic rooms, International Organization for Standardization, Switzerland, 2003.

[27] C. Boutin, P. Royer, J.L. Auriault, Acoustic absorption of porous surfacing with dual porosity, Int. J. Solids Struct., 35 (1998) 4709-4737.

[28] X. Olny, C. Boutin, Acoustic wave propagation in double porosity media, J. Acoust. Soc. Am., 114 (2003) 73-89.

[29] C. Boutin, R. Venegas, Assessment of the effective parameters of dual porosity deformable media, Mechanics of Materials, 102 (2016) 26-46.

[30] N. Atalla, R. Panneton, F.C. Sgard, X. Olny, Acoustic absorption of macro-perforated porous materials, J. Sound Vib., 243 (2001) 659-678.

[31] F.C. Sgard, X. Olny, N. Atalla, F. Castel, On the use of perforations to improve the sound absorption of porous materials, Appl. Acoust., 66 (2005) 625-651.

[32] M.E. Delany, E.N. Bazley, Acoustical properties of fibrous absorbent materials, Appl. Acoust., 3 (1970) 105-116.

[33] B. Nennig, Y. Renou, J.P. Groby, Y. Auregan, A mode matching approach for modeling two dimensional porous grating with infinitely rigid or soft inclusions, J. Acoust. Soc. Am., 131 (2012) 3841-3852.

[34] B.R. Mace, D. Duhamel, M.J. Brennan, L. Hinke, Finite element prediction of wave motion in structural waveguides, J. Acoust. Soc. Am., 117 (2005) 2835-2843.

[35] D.J. Mead, General theory of harmonic wave-propagation in linear periodic systems with multiple coupling, J. Sound Vib., 27 (1973) 235-260.

[36] L. Houillon, M.N. Ichchou, L. Jezequel, Wave motion in thin-walled structures, J. Sound Vib., 281 (2005) 483-507.

[37] J.M. Renno, B.R. Mace, On the forced response of waveguides using the wave and finite element method, J. Sound Vib., 329 (2010) 5474-5488.

[38] X. Sun, C. Zhou, M. Ichchou, J.P. Laine, A.M. Zine, Multi-scale homogenization of transversal waves in periodic composite beams, Int. J. Appl. Mech., 9 (2017) 30.

[39] D. Duhamel, B.R. Mace, M.J. Brennan, Finite element analysis of the vibrations of waveguides and periodic structures, J. Sound Vib., 294 (2006) 205-220.

[40] E. Manconi, B.R. Mace, Estimation of the loss factor of viscoelastic laminated panels from finite element analysis, J. Sound Vib., 329 (2010) 3928-3939.

[41] M.N. Ichchou, J. Berthaut, M. Collet, Multi-mode wave propagation in ribbed plates: Part I, wavenumber-space characteristics, Int. J. Solids Struct., 45 (2008) 1179-1195.

[42] Q. Serra, M.N. Ichchou, J.F. Deü, Wave properties in poroelastic media using a Wave Finite Element Method, J. Sound Vib., 335 (2015) 125-146.

[43] C. Jiang, C. Wang, L. Huang, Acoustic characterization of ducts lined with poroelastic materials based on wave finite element method, Appl. Acoust., 145 (2019) 362-373.

[44] J.M. Mencik, D. Duhamel, A wave-based model reduction technique for the description of the dynamic behavior of periodic structures involving arbitrary-shaped substructures and large-sized finite element models, Finite Elem. Anal. Des., 101 (2015) 1-14.

[45] C. Schaal, S. Bischoff, L. Gaul, Analysis of wave propagation in periodic 3D waveguides, Mech. Syst. Signal Proc., 40 (2013) 691-700.

[46] J.L. Auriault, C. Boutin, C. Geindreau, Homogenization of coupled phenomena in heterogenous media, John Wiley & Sons, 2010.

[47] H. Utsuno, T. Tanaka, T. Fujikawa, A.F. Seybert, Transfer-Function Method for Measuring Characteristic Impedance and Propagation Constant of Porous Materials, J. Acoust. Soc. Am., 86 (1989) 637-643.

[48] ISO, ISO 10534-2 Acoustics — Determination of sound absorption coefficient and acoustic impedance with the interferometer — Part 2: Transfer-function method, International Organization for Standardization, Switzerland, 1998.

[49] X. Zha, X. Zhou, H.V. Fuchs, Computer simulation and measurement of free-field characteristics, Audio Eng., 33 (2009) 6-13.

[50] P. Bonfiglio, F. Pompoli, Numerical methodologies for optimizing and predicting the low frequency behavior of anechoic chambers, J. Acoust. Soc. Am., 134 (2013) 285-291.

Appendix

A. Eigenvalue problem formulation with WFE method

The eigenvalue problem formulation approach with WFE method proposed by Mace et al. [34] is described as follows. The unit-cell of the PMV porous material is displayed in lower part of Fig. 1. With commercial finite element (FE) software COMSOL Multiphysics® , nodal motion equation of this unit is expressed as

$$\left(\mathbf{K}+\mathrm{i}\omega\mathbf{C}-\omega^2\mathbf{M}\right)\mathbf{q}=\mathbf{F}\,, \tag{A-1}$$

where **K**, **C** and **M** are the stiffness, damping and mass matrices, respectivly, **q** is the vector of nodal degree of freedoms (DOFs), and **F** is the vector of nodal forces. For this problem, the nodal DOFs is the acoustic pressure vector [p].

Introducing the dynamic stiffness matrix $\tilde{\mathbf{D}}=\mathbf{K}+\mathrm{i}\omega\mathbf{C}-\omega^2\mathbf{M}$ and dividing the nodal DOFs and nodal forces into left (L), right (R) cross-sections and internal (I) nodes, the equation of motion is partitioned as

$$\begin{bmatrix}\tilde{\mathbf{D}}_{II} & \tilde{\mathbf{D}}_{IL} & \tilde{\mathbf{D}}_{IR}\\ \tilde{\mathbf{D}}_{LI} & \tilde{\mathbf{D}}_{LL} & \tilde{\mathbf{D}}_{LR}\\ \tilde{\mathbf{D}}_{RI} & \tilde{\mathbf{D}}_{RL} & \tilde{\mathbf{D}}_{RR}\end{bmatrix}\begin{pmatrix}\mathbf{q}_I\\ \mathbf{q}_L\\ \mathbf{q}_R\end{pmatrix}=\begin{pmatrix}0\\ \mathbf{F}_L\\ \mathbf{F}_R\end{pmatrix}. \tag{A-2}$$

Eliminating $\mathbf{q}_I$ by the first line in the above equation,

$$\mathbf{q}_I=-\tilde{\mathbf{D}}_{II}^{-1}\left(\tilde{\mathbf{D}}_{IL}\mathbf{q}_L+\tilde{\mathbf{D}}_{IR}\mathbf{q}_R\right), \tag{A-3}$$

the motion equation for the left and right cross-section DOFs are obtained as

$$\begin{bmatrix}\mathbf{D}_{LL} & \mathbf{D}_{LR}\\ \mathbf{D}_{RL} & \mathbf{D}_{RR}\end{bmatrix}\begin{pmatrix}\mathbf{q}_L\\ \mathbf{q}_R\end{pmatrix}=\begin{pmatrix}\mathbf{F}_L\\ \mathbf{F}_R\end{pmatrix}, \tag{A-4}$$

where the new partitioned dynamic stiffness matrices are expressed as

$$\begin{cases}\mathbf{D}_{LL}=\tilde{\mathbf{D}}_{LL}-\tilde{\mathbf{D}}_{LI}\tilde{\mathbf{D}}_{II}^{-1}\tilde{\mathbf{D}}_{IL}\\ \mathbf{D}_{LR}=\tilde{\mathbf{D}}_{LR}-\tilde{\mathbf{D}}_{LI}\tilde{\mathbf{D}}_{II}^{-1}\tilde{\mathbf{D}}_{IR}\\ \mathbf{D}_{RL}=\tilde{\mathbf{D}}_{RL}-\tilde{\mathbf{D}}_{RI}\tilde{\mathbf{D}}_{II}^{-1}\tilde{\mathbf{D}}_{IL}\\ \mathbf{D}_{RR}=\tilde{\mathbf{D}}_{RR}-\tilde{\mathbf{D}}_{RI}\tilde{\mathbf{D}}_{II}^{-1}\tilde{\mathbf{D}}_{IR}\end{cases}. \tag{A-5}$$

Re-ordering Eq. (A-4), the transfer matrix formulation from the left cross-section to the right cross-section is obtained as

$$\mathbf{T}\begin{pmatrix}\mathbf{q}_L\\ \mathbf{F}_L\end{pmatrix}=\begin{pmatrix}\mathbf{q}_R\\ \mathbf{F}_R\end{pmatrix}, \tag{A-6}$$

where $\boldsymbol{T}$ is the transfer matrix,

$$\mathbf{T}=\begin{bmatrix} -\mathbf{D}_{LR}^{-1}\mathbf{D}_{LL} & \mathbf{D}_{LR}^{-1} \\ -\mathbf{D}_{RL}+\mathbf{D}_{RR}\mathbf{D}_{LR}^{-1}\mathbf{D}_{LL} & -\mathbf{D}_{RR}\mathbf{D}_{LR}^{-1} \end{bmatrix}. \tag{A-7}$$

Applying the periodic boundary condition, it is obtained that

$$\begin{pmatrix} \mathbf{q}_R \\ \mathbf{F}_R \end{pmatrix}=\lambda\begin{pmatrix} \mathbf{q}_L \\ \mathbf{F}_L \end{pmatrix}. \tag{A-8}$$

Combining Eqs. (A-6)and (A-8), the standard eigenvalue problem is formed as follows

$$\mathbf{T}\begin{pmatrix} \mathbf{q}_L \\ \mathbf{F}_L \end{pmatrix}=\lambda\begin{pmatrix} \mathbf{q}_L \\ \mathbf{F}_L \end{pmatrix}. \tag{A-9}$$

B. Equivalnet parameters calculation with finite unit

The following procedure is used to calculate the equivalent parameters of PMV porous materials with 5 units in COMSOL Multiphysics®. The calculation domain is shown in Fig. B-1.

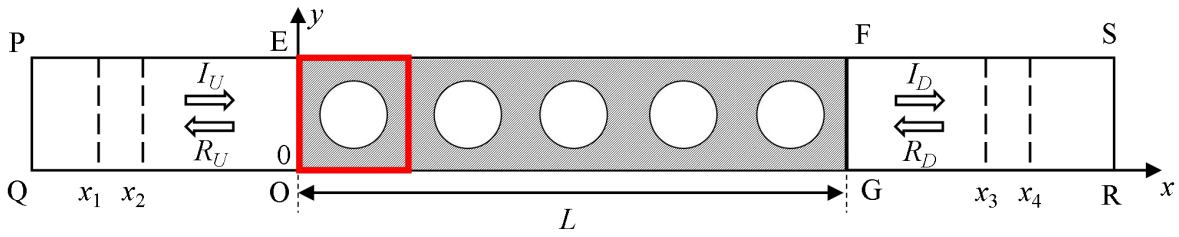

Fig. B-1. Calculation domain for equivalent parameters of PMV structure with 5 units.

In the upstream domain (PQOE), acoustic pressure p_U and horizontal component of particle velocity v_U are expressed as superposition of the incident wave $A_I\mathrm{e}^{-\mathrm{i}k_0x}$ and reflection wave $A_R\mathrm{e}^{+\mathrm{i}k_0x}$,

$$\begin{cases} p_U=A_I\mathrm{e}^{-\mathrm{i}k_0x}+A_R\mathrm{e}^{+\mathrm{i}k_0x} \\ v_U=\dfrac{1}{z_0}\left(A_I\mathrm{e}^{-\mathrm{i}k_0x}-A_R\mathrm{e}^{+\mathrm{i}k_0x}\right) \end{cases}, \tag{B-1}$$

with A_I and A_R being incident and reflection pressure amplitudes in the upstream. In the downstream domain (FGRS), acoustic pressure p_D and horizontal component of particle velocity v_D are expressed as superposition of the incident wave $B_I\mathrm{e}^{-\mathrm{i}k_0x}$ and reflection wave $B_R\mathrm{e}^{+\mathrm{i}k_0x}$,

$$\begin{cases} p_D=B_I\mathrm{e}^{-\mathrm{i}k_0x}+B_R\mathrm{e}^{+\mathrm{i}k_0x} \\ v_D=\dfrac{1}{z_0}\left(B_I\mathrm{e}^{-\mathrm{i}k_0x}-B_R\mathrm{e}^{+\mathrm{i}k_0x}\right) \end{cases}, \tag{B-2}$$

with B_I and B_R being incident and reflection pressure amplitudes in the downstream, respectively. The five-unit PMV domain (EOGF) is regarded as a special uniform medium with the equivalent characteristic impedance z_c and the equivalent wavenumber k_c. Therefore, the acoustic pressure p_M and horizontal component of particle velocity v_M inside the PMV porous material is assumed to be superposition of the incident wave $C_I e^{-ik_c x}$ and reflection wave $C_R e^{+ik_c x}$,

$$\begin{cases} p_M = C_I e^{-ik_c x} + C_R e^{+ik_c x} \\ v_M = \dfrac{1}{z_c}\left(C_I e^{-ik_c x} - C_R e^{+ik_c x} \right) \end{cases}, \tag{B-3}$$

with C_I and C_R being incident and reflection pressure amplitudes in the five-unit PMV porous material, respectively.

In the upstream, the averaged pressures over the dash lines $x=x_1$ and $x=x_2$ are calculated through line integration and referred to as p_1 and p_2 respectively. Hence, the linear equations for the unknown A_I and A_R are obtained as follows

$$\begin{cases} e^{-ik_0 x_1} A_I + e^{+ik_0 x_1} A_R = p_1 \\ e^{-ik_0 x_2} A_I + e^{+ik_0 x_2} A_R = p_2 \end{cases}. \tag{B-4}$$

Solving the above equations, the incident and reflection pressure amplitudes A_I and A_R in the upstream are obtained,

$$\begin{cases} A_I = \dfrac{p_1 e^{+ik_0 x_2} - p_2 e^{+ik_0 x_1}}{e^{ik_0 (x_2 - x_1)} - e^{ik_0 (x_1 - x_2)}} \\ A_R = \dfrac{p_2 e^{-ik_0 x_1} - p_1 e^{-ik_0 x_2}}{e^{ik_0 (x_2 - x_1)} - e^{ik_0 (x_1 - x_2)}} \end{cases}. \tag{B-5}$$

In the same way, in the downstream, incident and reflection pressure amplitudes (B_I and B_R) are obtained through standing wave decomposition for the two averaged pressures of p_3 (averaged over dash line $x=x_3$) and p_4 (averaged over dash line $x=x_4$),

$$\begin{cases} B_I = \dfrac{p_3 e^{+ik_0 x_4} - p_4 e^{+ik_0 x_3}}{e^{ik_0 (x_4 - x_3)} - e^{ik_0 (x_3 - x_4)}} \\ B_R = \dfrac{p_4 e^{-ik_0 x_3} - p_3 e^{-ik_0 x_4}}{e^{ik_0 (x_4 - x_3)} - e^{ik_0 (x_3 - x_4)}} \end{cases}. \tag{B-6}$$

With the calculated A_I, A_R, B_I and B_R, the averaged acoustic pressure and horizontal component of the particle velocity at boundary OE (line $x=0$) and FG (line $x=L$) are expressed as

$$\begin{cases} p_{x=0} = A_I + A_R \\ v_{x=0} = \dfrac{1}{z_0}\left(A_I - A_R\right) \\ p_{x=L} = B_I \mathrm{e}^{-\mathrm{i}k_0 L} + B_R \mathrm{e}^{+\mathrm{i}k_0 L} \\ v_{x=L} = \dfrac{1}{z_0}\left(B_I \mathrm{e}^{-\mathrm{i}k_0 L} - B_R \mathrm{e}^{+\mathrm{i}k_0 L}\right) \end{cases} . \tag{B-7}$$

In the five-unit PMV porous material domain, applying the continuity condition of pressure and normal component of particle velocity at boundaries OE and FG, the equations for C_I, C_R, k_c and z_c are obtained,

$$\begin{cases} C_I + C_R = p_{x=0} \\ \dfrac{1}{z_c}\left(C_I - C_R\right) = v_{x=0} \\ C_I \mathrm{e}^{-\mathrm{i}k_c L} + C_R \mathrm{e}^{+\mathrm{i}k_c L} = p_{x=L} \\ \dfrac{1}{z_c}\left(C_I \mathrm{e}^{-\mathrm{i}k_c L} - C_R \mathrm{e}^{+\mathrm{i}k_c L}\right) = v_{x=L} \end{cases} . \tag{B-8}$$

The equivalent characteristic impedance z_c and equivalent wavenumber k_c of the five-unit periodic waveguide is calculated by solving Eqs. (B-8),

$$\begin{cases} z_c = \sqrt{\dfrac{p_{x=L}^2 - p_{x=0}^2}{v_{x=L}^2 - v_{x=0}^2}} \\ k_c = -\dfrac{1}{\mathrm{i}L}\ln\left(\dfrac{p_{x=L} + v_{x=L} z_c}{p_{x=0} + v_{x=0} z_c}\right) \end{cases} . \tag{B-9}$$

The equivalent speed of sound (c_c) and density (ρ_c) are obtained by Eqs. (8) and (10).

Figure captions

Fig. 1. Geometry of the PMV porous material and its unit-cell.

Fig. 2. Mesh and pressure field (real part) [Pa] of fundamental mode for unit-cell of the PMV porous material at $f^* = 0.02$; (a) mesh; (b) pressure field.

Fig. 3. Convergence of calculated wavenumbers with mesh size S_e.

Fig. 4. Normalized equivalent density and bulk modulus of the PMV porous material with $R_f = 4000$ Pa·s/m^2 and macro porosity $\phi = 38.5\%$.

Fig. 5. Dispersion curve for fundamental mode of the PMV porous material with $R_f = 4000$ Pa·s/m^2 and macro porosity $\phi = 38.5\%$.

Fig. 6. Normalized equivalent density and bulk modulus of the PMV porous material validated by finite structure simulation with 5 units.

Fig. 7. Test sample of the PMV porous material, with macro porosity $\phi = 38.5\%$; (a) 3D view; (b) cross-sectional view.

Fig. 8. Normalized equivalent density and bulk modulus of the PMV porous material validated by experiments with macro porosity $\phi = 38.5\%$.

Fig. 9. Normalized equivalent density and bulk modulus of PMV porous materials with different macro void shapes.

Fig. 10. Normalized equivalent density and bulk modulus of PMV porous materials with change of void center position in at frequency $f^* = 0.02$; (a) density, void center change in x direction; (b) density, void center change in y direction; (c) bulk modulus, void center change in x direction; (d) bulk modulus, void center change in y direction.

Fig. 11. Normalized equivalent density and bulk modulus of PMV porous materials with change of macro porosity ϕ, at frequency $f^* = 0.02$; (a) equivalent density; (b) equivalent bulk modulus.

Fig. 12. Experimental results of sound absorption coefficient for uniform and gradient PMV porous materials with length of 0.4 m.

Fig. 13. Geometry for unit-cell of three-dimensional (3D) PMV design.

Fig. 14. Normalized equivalent density and bulk modulus of the 3D PMV porous material at different incident angles; line: $\theta = 0°$, $\beta = 0°$, circle marker: $\theta = 30°$, $\beta = 60°$.

Fig. 15. Oblique incidence sound absorption coefficient α of PMV absorbers with thickness of 0.1 m.